MAGNETISM
AND FERROELECTRICITY

Effect of Doping with Iron on the Charge Ordering
in $La_{0.33}Ca_{0.67}Mn_{1-y}Fe_yO_3$ ($y = 0, 0.05$) Manganites

T. S. Orlova[a, b], J.-Y. Laval[b], V. S. Zakhvalinskiĭ[c], and Yu. P. Stepanov[a]

[a] Ioffe Physicotechnical Institute, Russian Academy of Sciences, Politekhnicheskaya ul. 26, St. Petersburg, 194021 Russia
e-mail: orlova.t@mail.ioffe.ru
[b] Laboratoire de Physique du Solide, CNRS ESPCI, Paris, 75231 France
[c] Belgorod State University, ul. Pobedy 85, Belgorod, 308015 Russia
Received February 6, 2006

Abstract—The formation and specific features of the superstructure in $La_{0.33}Ca_{0.67}Mn_{1-y}Fe_yO_3$ ($y = 0, 0.05$) manganites doped with iron are investigated using transmission electron microscopy. The electron diffraction patterns of the manganites are studied in the temperature range 90–300 K, and the high-resolution electron microscope images recorded at temperatures of 91–92 K are analyzed. In both manganites, the structural transition that is accompanied by the formation of the superstructure and which is directly observed from the appearance of additional peaks in the electron diffraction patterns occurs at a temperature that is in close agreement with the charge ordering temperature T_{CO} determined from the temperature dependences of the magnetization $M(T)$. In the temperature range $90 < T < 200$ K, the undoped compound has a commensurate superstructure characterized by the vector $\mathbf{q} = 1/3\mathbf{a}^*$ and triple the unit cell $\langle\langle 3a \times b \times c \rangle\rangle$ (where $a \approx b \approx \sqrt{2}a_p$, $c \approx 2a_p$, and $a_p \sim 3.9$ Å is the lattice parameter of a simple perovskite). The doping with iron (5 at. %) brings about a decrease in the charge ordering temperature T_{CO} by 50 K and the formation of an incommensurate structure for which the magnitude of the vector $\mathbf{q}$ is smaller by approximately 15%. The unit cell of the superstructure in the iron-doped compound is not triple the unit cell but involves defects of ordering, such as quadrupling of the unit cell, numerous translations by $a_p\sqrt{2}$ along the **a** direction, and dislocation-type defects in the stripe structure of the charge ordering. These pseudoperiodic defects lead to a decrease in the magnitude of the vector $\mathbf{q}$ and are responsible for the incommensurability of the structure. A decrease in the charge ordering temperature T_{CO} due to the doping with iron and the incommensurability of the superstructure correlate with the change in the concentration of Mn^{3+} Jahn–Teller ions as a result of their replacement by Fe^{3+} non-Jahn–Teller ions.

PACS numbers: 75.47.Lx, 68.37.Lp

DOI: 10.1134/S1063783406110138

1. INTRODUCTION

Since the discovery of the giant magnetoresistance in $Ln_{1-x}Ae_xMnO_3$ compounds (where Ln is a lanthanide element and Ae is a divalent element), considerable research attention has been concentrated on the study of the many interesting properties of these perovskite materials [1–5]. The Ae concentration x can vary over a wide range ($0 \le x \le 1$). In this case, the physical properties of manganites change significantly because the system undergoes a number of phase transitions accompanied by a change in ordering of different types, such as magnetic, structural, and electronic ordering. The majority of experimental and theoretical works have predominantly dealt with investigating the properties of manganites in the concentration range $0 < x < 0.5$. In materials with these compositions, holes in the split e_g band of manganese play the role of free carriers. Manganites belonging to the above region of the phase diagram possess a unique property, i.e., negative giant magnetoresistance, which manifests itself in a

severalfold decrease in the electrical resistivity in response to an applied magnetic field. The maximum effect is observed at temperatures close to the temperature T_C (where T_C is the Curie temperature) of the transition from a paramagnetic dielectric state to a ferromagnetic metallic state. The metal–insulator transition and the giant magnetoresistance effect at temperatures close to the temperature T_C can be qualitatively explained by the simultaneous presence of Mn^{3+} and Mn^{4+} ions in manganites of these compositions and by the mechanism of double exchange of electrons between these ions (Mn^{4+}–O–Mn^{3+}) through the intermediate oxygen atom [6, 7].

In a number of papers (see, for example, [8]), it has been emphasized that, in manganites, the special role is played both by the electron–phonon interactions associated with the Jahn–Teller distortion of the environment of Mn^{3+} ions and by the experimentally observed phase separation [9, 10], which indicates the formation

of a magnetically inhomogeneous structure on the microscopic level.

The manganites $Ln_{1-x}Ae_x$MnO$_3$, which correspond to another region of the phase diagram at $x > 0.5$, undergo a transition to a charging ordering (CO) state: at low temperatures, these materials become antiferromagnetic insulators characterized by charge ordering [11–13]. The possibility of the charge ordering that occurs at the transition temperature T_{CO} and has a non-magnetic nature was originally noted by Goodenouph [11] in respect to the superstructure peaks revealed in neutron diffraction investigations not related to magnetism [14]. Goodenouph offered a qualitative explanation for this phenomena based on mutual ordering of the Mn^{3+} and Mn^{4+} ions. The charge ordering is closely associated with the orbital ordering due to the Jahn–Teller distortion of Mn^{3+}O$_6$ octahedra: the $d(z^2)$(Mn^{3+}) orbitals are oriented perpendicular to the c axis and form a series of oriented chains in the $(a–b)$ plane. This lattice distortion can be clearly observed in transmission electron microscope images recorded along the c axis. In the LaCaMnO manganites, the stripe structure caused by the charge ordering was observed in [15, 16]. However, the obtained images had a poor atomic resolution due to the mechanical instability of the samples at low temperatures and, therefore, could not be used to reveal specific features of the structural ordering.

In recent years, researchers have focused particular attention on studying the charge ordering phenomenon in $Ln_{0.5}Ae_{0.5}$MnO$_3$ manganites [10, 17–21]. It has been demonstrated that, in these systems, there exists a close interrelationship between the spin, charge, and orbital orderings responsible for the magnetic and transport properties. Unfortunately, this interrelationship is still not clearly understood. These materials represent a special case, because the competition between two types of magnetic ordering (i.e., the ferromagnetic metallic and antiferromagnetic insulating orderings) is observed in a narrow region of the phase diagram in the vicinity of $x = 0.5$ (Mn^{3+}: Mn^{4+} = 1). Furthermore, since these compounds are very sensitive to a variation in the oxygen content [18, 22], even an insignificant change in the oxygen content can lead to a shift from the hole-doped region to the electron-doped region of the phase diagram and vice versa. From this standpoint, the $Ln_{1-x}Ae_x$MnO$_3$ manganites at $x > 0.5$ are less sensitive to a variation in the oxygen content, because they are located farther from the ferromagnetic–antiferromagnetic boundary in the phase diagram. It should be noted that the structure and properties of these manganites are considerably less well understood. The so-called commensurate compounds La$_{0.33}$Ca$_{0.67}$MnO$_3$ (Mn^{3+} : Mn^{4+} = 1/2) and La$_{0.25}$Ca$_{0.75}$MnO$_3$ (Mn^{3+} : Mn^{4+} = 1/3) are of special interest. In these compounds, Mori et al. [23] found stripes comprising a regular alternation of structural units formed predominantly by chains of Mn^{3+}

Jahn–Teller ions and structural units composed only of chains consisting of Mn^{4+} ions [23, 24].

At present, the mechanism of charge ordering is not clearly understood, because this process leads to simultaneous ordering of charges, spins, and orbitals of Mn^{3+} and Mn^{4+} ions. In order to gain better insight into the charge ordering, it is expedient to investigate materials doped with impurity elements. Light doping with different elements substituting for Mn sites can bring about a considerable change in the physical properties of manganites, as is the case with application of a magnetic field [25], pressure [26], or other actions. Most likely, all these phenomena are closely related to each other and the results of investigation into the doping of Mn sites can play a key role in understanding their nature. For example, the insulator–metal transition was revealed in Pr$_{0.5}$Ca$_{0.5}$Mn$_{1-y}$Cr$_y$O$_3$ manganites in the absence of a magnetic field [19, 20]. The doping of the La$_{0.3}$Ca$_{0.7}$Mn$_{0.8}$Cr$_{0.2}$O$_3$ manganite with chromium leads to the suppression of charge ordering and to the appearance of magnetoresistance. All the above facts suggest that the phase diagram of manganites can be substantially modified by doping these compounds at Mn^{3+} sites with magnetic cations.

The effect of doping with iron on the charge ordering is also of interest because of the following reasons: (i) the Fe^{3+} ions have a radius identical to that of Mn^{3+} ions; (ii) the Fe^{3+} ions are magnetic cations but are non-Jahn–Teller cations; and (iii) the Fe^{3+} ions, unlike Cr^{3+} ions, do not participate in the double exchange [27, 28]. The effect of the doping with iron on the electrical and magnetic properties was studied primarily in hole-doped manganites La$_{1-x}$Ca$_x$Mn$_{1-y}$Fe$_y$O$_3$ (x = 0.30, 0.25) [27, 29]. It was demonstrated that, in these materials, the Fe^{3+} ions substitute for Mn^{3+} ions and do not provide ferromagnetic interaction through the Fe^{3+}–Mn^{4+} double exchange.

The effect of doping with iron on the temperature dependences of the magnetization and the electrical resistivity has been studied for the La$_{0.5}$Ca$_{0.5}$MnO$_3$ manganite with the boundary composition in the phase diagram [28, 30]; however, the data obtained are contradictory. Since, as was noted above, compounds with a La : Ca ratio close to the ratio La : Ca = 1 are very sensitive to the oxygen content, even a very insignificant variation in the oxygen content can very strongly affect their physical properties [22]. Most likely, this circumstance explains the contradictoriness of the results obtained.

It should be noted that the effect of doping with iron on the charge ordering of manganites with the initial composition corresponding to the antiferromagnetic insulating state ($x > 0.5$) has not been systematically investigated to date. Moreover, the influence of the doping on the structure of LaCaMnFeO manganites of any composition has never been examined using transmission electron microscopy (TEM), even though this

method allows one to observe the formation of superstructures directly and to study their specific features.

In this work, the effect of doping with iron on the formation of the superstructure in polycrystalline samples of $La_{0.33}Ca_{0.67}Mn_{1-y}Fe_yO_3$ ($y = 0, 0.05$) was investigated by analyzing the electron diffraction patterns in the temperature range 90–300 K and high-resolution electron microscope lattice images obtained at low temperatures. The structural investigations were accompanied by studying the physical properties, magnetization, and electrical resistivity.

2. SAMPLE PREPARATION AND EXPERIMENTAL TECHNIQUE

Samples of $La_{0.33}Ca_{0.67}Mn_{1-y}Fe_yO_3$ ($y = 0, 0.5$) manganites were synthesized by the solid-phase reaction (see, for example, [12]) from the initial oxides La_2O_3, $CaCO_3$, MnO_2, and Fe_2O_3, which were mixed in specified stoichiometric proportions and annealed two times in air at a temperature of 1320 K for 35 h with intermediate milling. The prepared powders were pressed in the form of rectangular parallelepipeds 7 × 7 × 4 mm in size under uniform compression at a pressure of 30 MPa. Final annealing was performed in air at 1375°C for 22 h.

The synthesized samples were characterized by x-ray powder diffraction analysis on a Philips automated x-ray diffractometer (CuK_α radiation).

The structure was investigated by the analyzing electron diffraction patterns recorded at different temperatures (step, 10–12 K; temperature range, 91–300 K) and bright-field and dark-field high-resolution electron microscope images recorded at temperatures of 91–92, 140, and 300 K with a Jeol 2010 F transmission electron microscope (voltage, 200 kV) equipped with a field emission gun. The sample was placed in a special low-temperature holder cooled with liquid nitrogen. The holder made it possible to vary and maintain a specified temperature in the range 90–300 K and to change the inclination of the sample by ±30° in two coordinates.

The electron microscope images were analyzed using the direct and inverse Fourier transforms with the Digital Micrograph program package and a special laboratory program (Industrial Physics and Chemistry Higher Educational Institution, Paris). The chemical composition of the samples was determined locally in situ with the use of an energy dispersive x-ray (EDX) analyzer mounted in an electron microscope. The size of the EDX probe was 1–2 nm. The oxygen content in the samples was examined by iodometric titration (see, for example, [31]).

The samples for electron microscopic investigations were mechanically polished to a thickness of approximately 20–30 μm and then were thinned to electron transparency (≤50 nm) with an argon gun.

Table 1. Lattice parameters $a \approx b$ and c determined by x-ray diffraction analysis for the undoped and iron-doped (5 at. % Fe) samples

Sample	a, Å	c, Å
$La_{0.33}Ca_{0.67}MnO_3$	5.360	7.609
$La_{0.33}Ca_{0.67}Mn_{0.95}Fe_{0.05}O_3$	5.364	7.580

The electrical resistivity of the samples 2.0 × 0.5 × 8.0 mm in size was measured by the conventional four-point probe method in the temperature range 6–300 K during cooling and heating.

The temperature dependences of the magnetization $M(T)$ in the temperature range 4.2–400 K was measured on a quantum SQUID magnetometer after cooling of the sample to 4.2 K in a zero magnetic field or different dc magnetic fields.

3. RESULTS AND DISCUSSION

According to the x-ray diffraction data, both compounds under investigation have an orthorhombic perovskite structure of the *Pbnm* type with the lattice parameters $a \approx b \approx \sqrt{2}a_p$ and $c \approx 2a_p$ (where $a_p \sim 3.9$ Å is the lattice parameter of a simple perovskite [16]) without any impurity phases or precipitations of pure iron. The lattice parameters obtained for the doped and undoped compounds according to the x-ray diffraction data are listed in Table 1. It can be seen from this table that the doping does not lead to a noticeable change in the lattice parameters. Most likely, this is associated with the substitution of Fe^{3+} ions for Mn^{3+} ions that, as was noted in Introduction, possess identical ionic radii.

Moreover, the chemical composition was controlled using EDX analysis (ultrafine probe, 1–2 nm) directly in the electron microscope. For this purpose, the ratio La : Ca : Mn and the iron distribution were determined at different points inside an individual grain and in 10–15 different grains and the concentration profiles across several grain boundaries were measured in order to check possible grain-boundary segregation of iron.

The EDX data obtained for the initial sample confirm a high chemical homogeneity of individual grains: the La : Ca ratios at different points of the grain differ by less than 3%. This virtually corresponds to the error in the measurements. However, the analysis of different grains indicates that the homogeneity is somewhat lower: the La : Ca ratio varies from 0.31 to 0.34 and, on average, is equal to 0.33 for the sample as a whole.

In the doped samples, the change in the La : Ca ratio within individual grains does not exceed 3%. For different grains, this ratio varies over a wider range from 0.31 to 0.35 and, on average, is equal to 0.33 for the whole sample, as is the case with the initial sample. The iron content amounts to 5% of the (Mn + Fe) atomic content in all the grains under investigation. No iron segrega-

Table 2. Results of iodometric titration

Sample	Oxygen content $(3 - \delta)$
$La_{0.33}Ca_{0.67}MnO_{3-\delta}$	2.966
$La_{0.33}Ca_{0.67}Mn_{0.95}Fe_{0.05}O_{3-\delta}$	2.964

tion in grain boundaries is observed. Since the probe size used in EDX analysis is very small, the inference can be made that iron is uniformly distributed over the samples.

The oxygen content in the samples under investigation was controlled by iodometric titration. The results obtained are presented in Table 2. As can be seen from this table, the oxygen content is virtually identical in the initial and doped materials, even though in both cases it differs slightly from the oxygen content corresponding to the chemical formula.
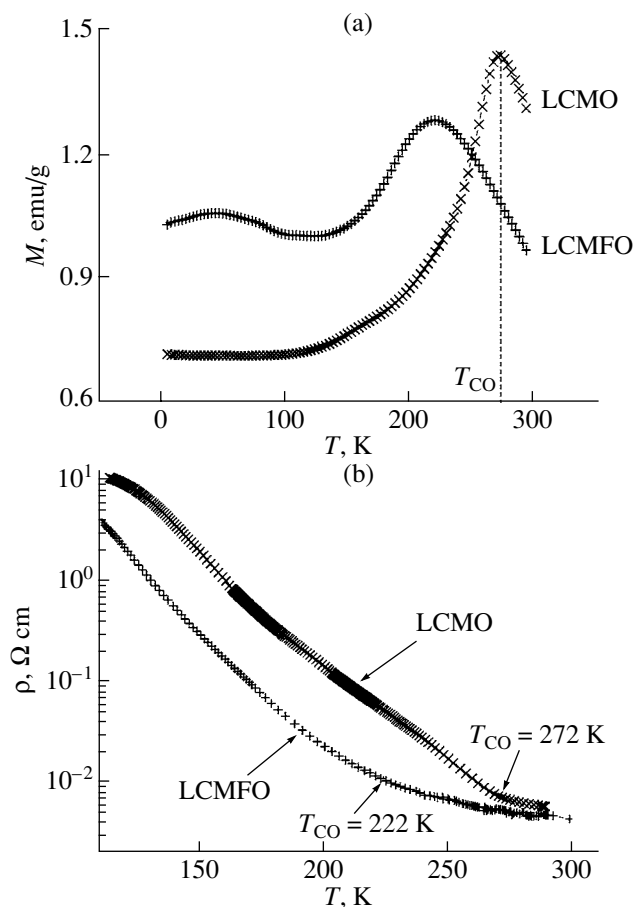
Fig. 1. (a) Temperature dependences of the magnetization M for $La_{0.33}Ca_{0.67}MnO_3$ and $La_{0.33}Ca_{0.67}Mn_{0.95}Fe_{0.05}O_3$ compounds in the magnetic field $H = 1$ T after preliminary cooling in a zero magnetic field to $T = 4.2$ K. (b) Temperature dependences of the electrical resistivity for the $La_{0.33}Ca_{0.67}MnO_3$ and $La_{0.33}Ca_{0.67}Mn_{0.95}Fe_{0.05}O_3$ compounds.

Figure 1a shows the temperature dependences of the magnetization M for the initial ($La_{0.33}Ca_{0.67}MnO_3$) and iron-doped ($La_{0.33}Ca_{0.67}Mn_{0.95}Fe_{0.05}O_3$) samples in the magnetic field $H = 1$ T after preliminary cooling in a zero magnetic field to liquid-helium temperature. As is well known for similar compounds, the magnetization peak observed at $T_{CO} \approx 272$ K for the initial sample is associated with the transition from the paramagnetic state to the charge-ordered state. The transition temperature $T_{CO} \approx 272$ K determined for the initial sample is in good agreement with the data available in the literature. In particular, the temperature $T_{CO} = 260$ K of the transition to the charge-ordered state in the $La_{0.3}Ca_{0.7}MnO_3$ compound was obtained from the peak in the dependence $M(T)$ by Sudyoadsuk et al. [21]. The transition temperature $T_{CO} = 270$ K for the $La_{0.333}Ca_{0.667}MnO_3$ compound was determined from the neutron powder diffraction data by Radeaelli et al. [32].

The temperature dependence of the magnetization $M(T)$ for the iron-doped $La_{0.33}Ca_{0.67}Mn_{0.95}Fe_{0.05}O_3$ sample is similar to that of the initial sample. However, the magnetization peak is observed at the temperature $T_{CO} = 222$ K, i.e., 50 K lower than in the case of the undoped material (Fig. 1a). It will be shown below that, this peak, as for the undoped compound, is attributed to the transition to the charge-ordered state.

The temperature dependences of the electrical resistivity for both compounds under investigation are plotted in Fig. 1b. The doping with 5 at. % Fe does not affect the behavior of the temperature dependence of the resistivity. It can be seen from Fig. 1b that, as the temperature decreases, the resistivity increases drastically beginning with the temperature T_{CO} (specific for the initial and iron-doped samples). This is explained by the change in the conduction mechanism due to the charge ordering [33]. The charge transfer occurs between Mn^{3+} and Mn^{4+} ions [34]. The charge ordering leads to a change in the electronic configuration of manganese ions [34]. This, in turn, results in a change in the conduction mechanism. Note that the temperature of the sharp increase in the resistivity of the iron-doped sample is approximately 50 K below the corresponding temperature for the undoped sample. This agrees well with the transition temperature T_{CO} determined from the magnetic measurements.

On the structural level, the influence of the doping with iron on the charge ordering was investigated with the use of electron microscopy by analyzing the evolution of the electron diffraction patterns with variations in temperature and the high-resolution lattice images obtained at low temperatures.

The electron diffraction patterns of the initial and iron-doped samples at room temperature are typical of the *Pbnm* orthorhombic structure (Fig. 2a). However, the electron diffraction patterns measured at 91 K exhibit an additional system of reflections located

between the main Bragg peaks (Fig. 2b). These additional satellite reflections are attributed to the superstructure formed as a result of the charge ordering and can be indexed in the traditional system as $\mathbf{q} = (1/3 - \varepsilon)\mathbf{a}^*$, where ε is the incommensurability parameter ($\varepsilon = 0$ in Fig. 2b). The formation of similar structures for the $La_{0.33}Ca_{0.67}MnO_3$ initial compound is known in the literature (see, for example, [16, 23]).

For each compound under investigation, we studied electron diffraction in approximately 15 grains with different orientations, i.e., with different systems of diffracting planes. It was revealed that the charge ordering is observed throughout the sample in the case of both the initial and iron-doped compounds.

At a low temperature, the initial sample is characterized by charge ordering with the vector $\mathbf{q}$ equal to $1/3\mathbf{a}^*$. The difference between the magnitudes of the vector $\mathbf{q}$ in different grains does not exceed 5%, which is within the limits of experimental error. Therefore, we can make the inference that the charge ordering in the initial sample at a low temperature $T = 91$–92 K is commensurate: the parameter of the newly formed superstructure along the direction $\mathbf{a}$ is equal to triple the lattice parameter $3a$.

In the iron-doped sample, the magnitude of the vector $\mathbf{q}$ at a temperature $T = 91$–92 K varies from 0.28 to 0.31 in different grains, as well as at different points within the same grain. Moreover, the mean magnitude of the vector $\mathbf{q}$ in the doped sample is approximately 15% less than that in the undoped sample. Consequently, the charge ordering in the iron-doped sample is incommensurate; i.e., the ratio between the magnitude of the vector $\mathbf{q}$ and the reciprocal lattice parameter a^* cannot be represented as the first numbers of a natural series. In order to elucidate the specific features of the superstructure, we obtained the high-resolution electron microscope lattice images, which will be discussed below.

Van Tendeloo et al. [17] noted that the temperature determining the $Mn^{3+} : Mn^{4+}$ ratio, the La : Ca ratio, and the oxygen content at a given value of x, which also affects the $Mn^{3+} : Mn^{4+}$ ratio, are the most important parameters of the charge ordering in $La_{1-x}Ca_xMnO_3$ compounds. According to Chen et al. [16], $La_{1-x}Ca_xMnO_3$ compounds are characterized by the relationship $q \sim (1 - x)$.

As was shown above, the EDX data obtained for the initial and doped samples indicate that the La : Ca ratios are identical for both samples. As follows from the iodometric titration data, the oxygen contents in the initial and doped compounds are also virtually the same (Table 2). Consequently, the substitution of Fe^{3+} ions for Mn^{3+} ions is the sole factor responsible for the change in the $Mn^{3+} : Mn^{4+}$ ratio in our case.

The ratio between the manganese ions in different charge states in the initial compound is $Mn^{3+} : Mn^{4+} = 1 : 2$, whereas the corresponding ratio in the doped
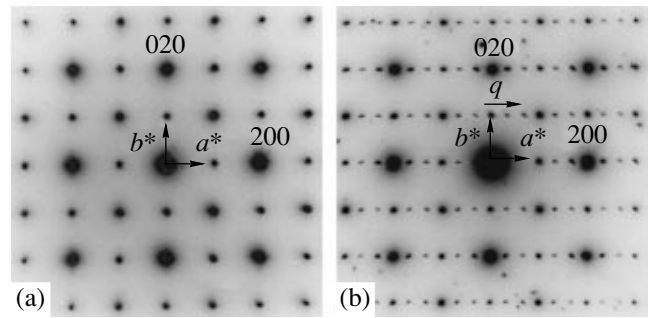
Fig. 2. Electron diffraction patterns of the $La_{0.33}Ca_{0.67}MnO_3$ compound (in the zone with the [001] normal) at (a) room temperature and (b) 91 K. Clear but weaker satellite reflections with the vector $\mathbf{q} = 1/3\mathbf{a}^*$ correspond to the superstructure formed upon charge ordering.
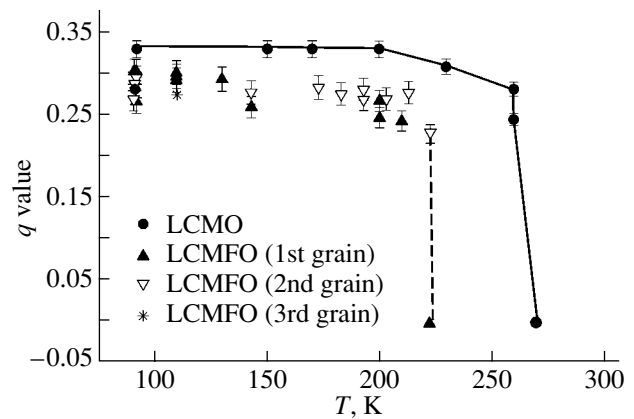
Fig. 3. Temperature dependences of the magnitude of the vector $\mathbf{q}$ for $La_{0.33}Ca_{0.67}MnO_3$ and $La_{0.33}Ca_{0.67}Mn_{0.95}Fe_{0.05}O_3$ compounds.

material with 5 at. % Fe is $Mn^{3+} : Mn^{4+} = 0.85 : 2$. This corresponds to a decrease in the $Mn^{3+} : Mn^{4+}$ ratio by 15% and is in agreement with the difference between the magnitudes of the vector $\mathbf{q}$ in the doped and initial compounds.

Let us consider how the temperature affects the selected-area electron diffraction from the $(00l)$ basal planes for specific crystal regions (grains). The measurements were performed for different grains in the initial and doped samples. The temperature was varied from 90 to 300 K in steps of 10–20 K. At each temperature, the electron diffraction patterns were recorded for identical electron beam parameters and the same exposure time.

The temperature dependences of the magnitude of the vector $\mathbf{q}$ for the initial and doped compounds are shown in Fig. 3. As can be seen from this figure, the magnitude of the vector $\mathbf{q}$ for the initial sample is equal to $1/3$ at 91 K and remains unchanged to temperatures $T_{plat} \sim 170$–200 K with an increase in the temperature. Schuddinck et al. [18] observed a similar behavior,

Fig. 4. Evolution of the satellite reflections with the vector $\mathbf{q} = (1/3 - \varepsilon)\mathbf{a}^*$ in the electron diffraction patterns of the $La_{0.33}Ca_{0.67}Mn_{0.95}Fe_{0.05}O_3$ compound during a step-by-step increase in temperature. Arrows indicate residual diffuse smearing of the satellite reflections.

ples without oxygen deficiency. In [18], the temperature T_{plat} was identified with the Néel temperature T_N corresponding to the formation of an antiferromagnetic structure of the CE type [18]. However, in our case (Fig. 3), the magnitude of the vector $\mathbf{q}$ does not sharply decrease at a particular temperature T_{plat}. We can only note a tendency toward an insignificant decrease in the magnitude of the vector $\mathbf{q}$ in different grains beginning with a temperature in the range 170–200 K. With a further increase in the temperature, a weak decrease in the magnitude of the vector $\mathbf{q}$ gives way to a drastic decrease in a narrow temperature range 260–270 K. This is accompanied by a considerable decrease in the intensity of the satellite reflections, which become diffuse and virtually disappear at $T \approx 270$ K. Therefore, the temperature of the observed structural transition $T \approx 270$ K agrees well both with the temperature T_{CO} determined from the magnetic measurements and with the temperature dependence of the electrical resistivity.

As for the initial compound, the quantity q for the doped compound initially remains almost constant with an increase in the temperature (Fig. 3). However, the satellite peaks become diffuse along the $\mathbf{a}^*$ direction beginning with a temperature of approximately 200 K. The pronounced superstructure peaks disappear at a temperature of approximately 220 K, which is approximately 50 K below the temperature T_{CO} for the initial sample. Therefore, the temperature dependence of the quantity $q(T)$ is in good agreement with the characteristic temperature revealed for the charge ordering from the temperature dependence of the magnetization $M(T)$. However, the electron diffraction patterns of the doped samples exhibit a characteristic feature in the form of residual diffuse smearing (streaking) along the $\mathbf{a}^*$ direction up to temperatures of 240–250 K, i.e., at temperatures substantially higher than the temperature T_{CO}. It should be noted that diffuse streaking was observed not throughout the sample (grain) but only in a number of nanoregions and the electron diffraction patterns of the remaining regions of the grain did not exhibit similar manifestations of the charge ordering at these temperatures. The evolution of the electron diffraction patterns of the doped compound with variations in temperature is illustrated in Fig. 4. The arrows indicate residual diffuse smearing of the satellites at temperatures $T > T_{CO}$. This residual diffuse smearing of the satellite peaks most likely suggests that a partial charge ordering (insignificant and in separate small regions) is retained to temperatures considerably higher than the temperature T_{CO}. These structural features cannot be revealed from the results of magnetic measurements.

In order to gain a deeper insight into the influence of iron on the charge ordering process and specific features of formation of the incommensurate superstructure in the doped sample, we performed high-resolution electron microscopic investigations of the initial and doped compounds at room and low ($T = 91$–92 and 140 K) temperatures.

namely, the presence of a plateau in the temperature dependence of the magnitude of the vector $\mathbf{q}$ with a plateau temperature $T_{plat} = 160$ K for $La_{0.5}Ca_{0.5}MnO_3$ sam-
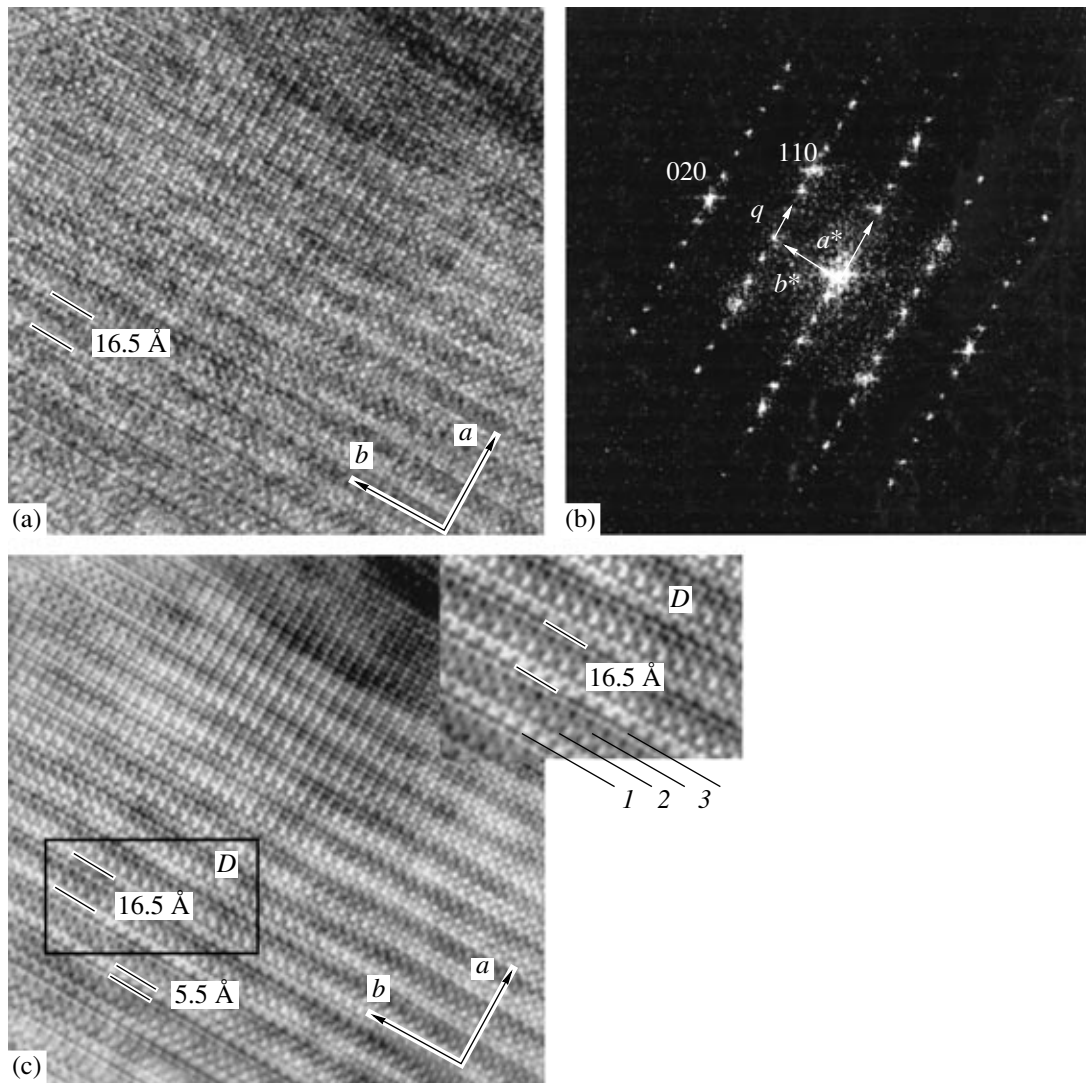
Fig. 5. (a) High-resolution lattice image of the La$_{0.33}$Ca$_{0.67}$MnO$_3$ compound at a temperature of 91 K. The observed superstructure is characterized by a periodicity of 16.5 Å = 3a. (b) Electron diffraction pattern obtained by the direct Fourier transform of the image displayed in panel (a). (c) Image obtained by the inverse Fourier transform of the electron diffraction pattern shown in panel (b). The inset presents region D on an enlarged scale with alternating fringes *1–3* forming the superstructure unit.

Figure 5a displays the typical high-resolution electron microscope lattice image of the initial sample along the [001] direction at a temperature of 91 K. Conventional image processing by filtering was used in order to enhance the image contrast. The Fourier transform of the image displayed in Fig. 5a is shown in Fig. 5b. Then, all the reflections (including the main and satellite reflections) visible in the calculated diffraction pattern in Fig. 5b were separated with the use of a special mask. Thereafter, we performed the inverse Fourier transform, which is shown in Fig. 5c. It can be seen that the images in Figs. 5a and 5c exhibit a regular fringe pattern of the (00*l*) planes, in which one bright fringe 5.5 Å in width (inset to Fig. 5c, fringe *1*) alternates with two neighboring, less bright fringes (inset to Fig. 5c, fringes *2*, *3*) with approximately the same

width. This regular fringe pattern has one characteristic size that is approximately equal to 16.5 Å, corresponds to triple the lattice parameter $3a \approx 3a_p\sqrt{2}$, and agrees with the magnitude of the vector **q** = 1/3**a*** in reciprocal space. According to [16, 17, 23], the observed superstructure corresponds to the expected 1 : 2 ordering of chains formed by Jahn–Teller strongly distorted Mn^{3+}O$_6$ octahedra and chains composed of undistorted Mn^{4+}O$_6$ octahedra. This regular structural ordering was observed at low temperatures throughout the crystal (grain) or transformed into twin ordering in crystals containing twins. The Jahn–Teller nature of these stripe structures with charge and orbital ordering was discussed in more detail in [10, 23, 24]. It should be noted that no indications of the superstructure in either the initial or doped compounds were observed in the high-
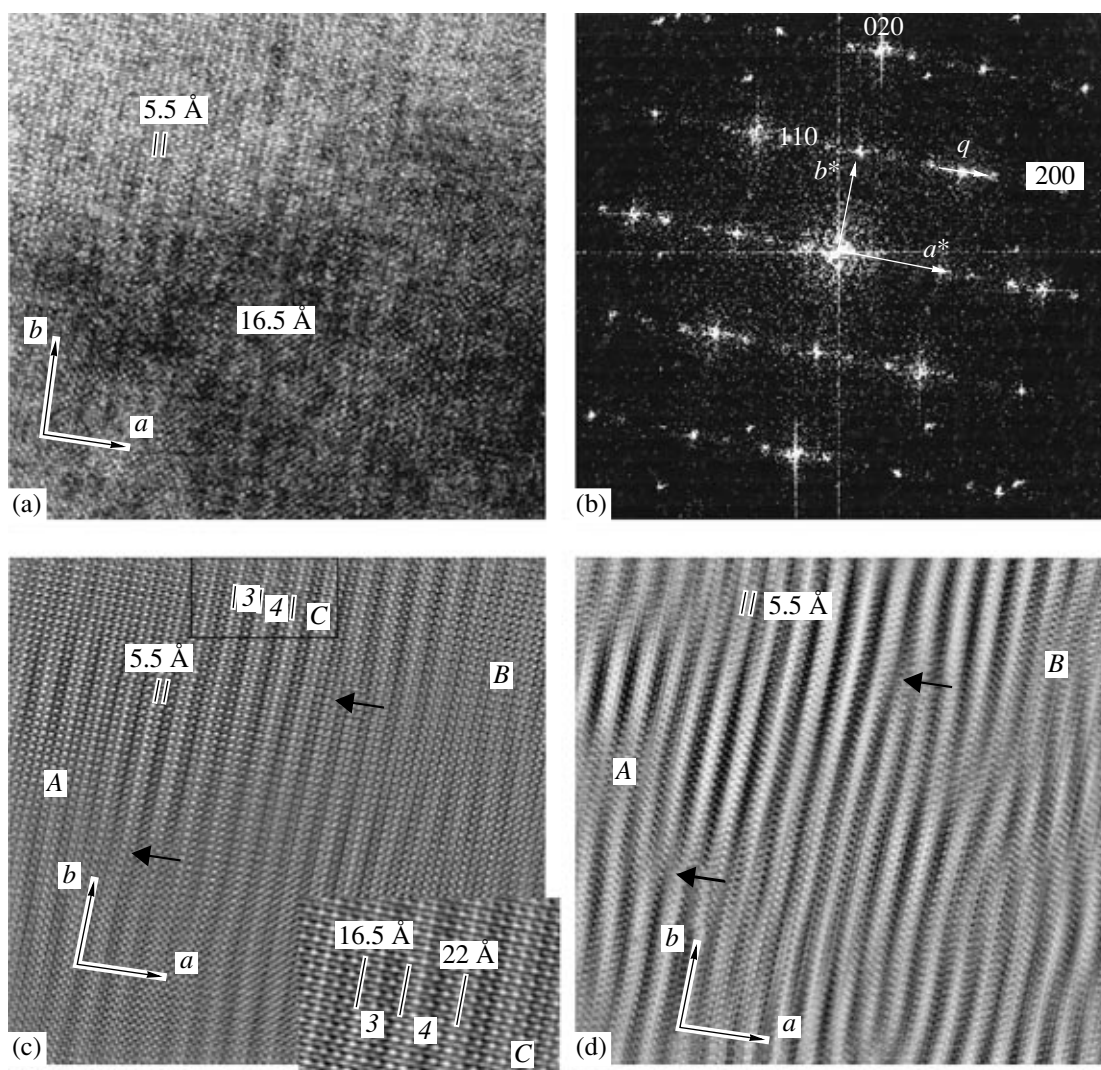
Fig. 6. (a) High-resolution electron microscope image of the $La_{0.33}Ca_{0.67}Mn_{0.95}Fe_{0.05}O_3$ compound at a temperature of 91 K. (b) Electron diffraction pattern obtained by the direct Fourier transform of the image displayed in panel (a). (c) Image obtained by the inverse Fourier transform of the electron diffraction pattern shown in panel (b). The inset presents region C on an enlarged scale with examples of local changes in the superstructure periodicity that correspond to triple the unit cell and quadruple the unit cell. (d) Image obtained by the inverse Fourier transform of the electron diffraction pattern displayed in panel (b) with due regard only for the separated satellite reflections.

resolution electron microscope lattice images measured at room temperature.

The high-resolution electron microscope image obtained at 91 K for the sample doped with 5 at. % Fe is displayed in Fig. 6a. The direct (Fig. 6b) and inverse (Fig. 6c) Fourier transforms were obtained according to the above procedure. Moreover, an additional inverse Fourier transform was performed only with the use of the satellite reflections separated in Fig. 6b by a special mask in order to construct the image of the superstructure (Fig. 6d). The image of the crystal with the $q = 1/3 - \varepsilon$ ($\varepsilon \approx 0.05$) for the iron-doped sample also exhibits a fringe pattern. However, it is clearly seen that the sequence of bright and less bright fringes is substantially less regular than the corresponding sequence for

the undoped sample. It is evident that iron strongly distorts the regular superstructure.

The main features revealed in the superstructure formed in the iron-doped compound can be summarized as follows.

(i) The sequence of bright and less bright fringes is considerably less regular than the corresponding sequence for the undoped sample. The distance between bright fringes separated by two less bright fringes, as before, is approximately equal to 16.5 Å ($\approx 3a_p\sqrt{2}$) and corresponds to triple the lattice parameter a. This fringe arrangement alternates with a number of other structural units. In the most typical units, three less bright fringes are located between two single bright fingers. This corresponds to the structural unit $4a_p\sqrt{2}$ (Fig. 6c).
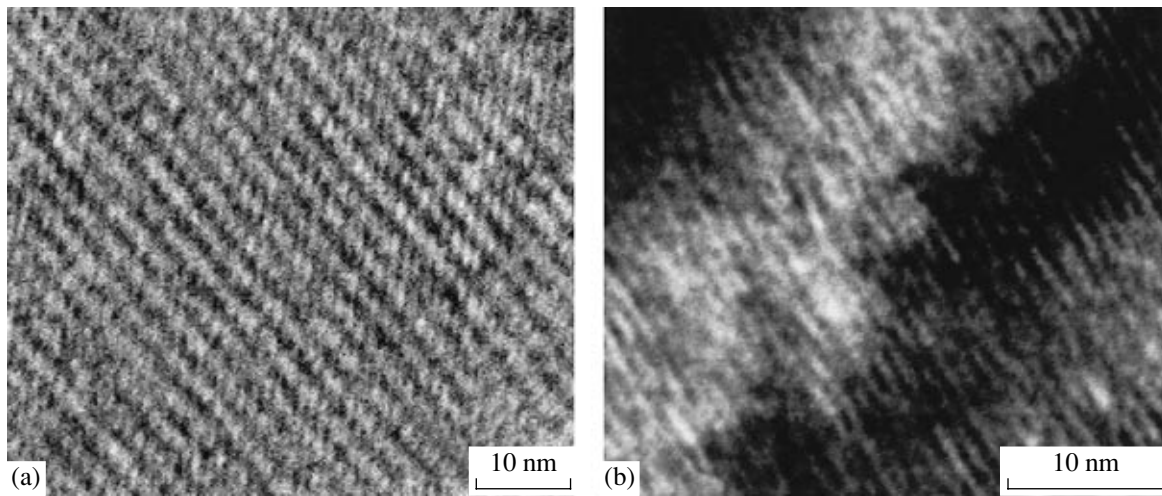
Fig. 7. High-resolution electron microscope images of the $La_{0.33}Ca_{0.67}MnO_3$ and $La_{0.33}Ca_{0.67}Mn_{0.95}Fe_{0.05}O_3$ compounds at a temperature of 91 K.

(ii) Furthermore, there are shifts of fringes along the **a** direction. These shifts are indicated in Fig. 6c by black arrows at the points where the bright fringe goes into the less bright fringe. The corresponding translation is equal to $a_p\sqrt{2}$. Similar shifts were observed in a number of other manganites, for example, in the $Nd_{0.5}Ca_{0.5}Mn_{1-y}Cr_{1-y}O_3$ system [18].

(iii) The observed stripe structure of the charge ordering is characterized by defects of the dislocation type. A number of these defects are clearly seen in the vicinity of the black arrows in Figs. 6c and 6d. The formation of these defects is most likely associated with the presence of Fe^{3+} ions. This leads to the so-called impurity effect (pinning of superstructure discommensurations). The pinning effect associated with the Ru impurities in the SmCaMnRuO system was noted by van Tendeloo et al. [17].

Therefore, the defects observed in the stripe structure of the charge ordering bring about the incommensurability of this structure and, as a consequence, a decrease in the quantity q for the iron-doped compound. Numerous shifts in stripes and dislocation-type defects of the stripe structure are responsible for the wavy shape of the charge-ordering stripes and the formation of nanoregions (for example, regions A and B in Figs. 6c and 6d) with a considerably less pronounced charge ordering. Figure 7b displays the high-resolution electron microscope image of the stripe structure of the doped sample at a lower magnification. It can be clearly seen from this figure that the stripes in the newly formed superstructure have a wavy shape, whereas straight-line stripes are observed for the undoped sample (Fig. 7a).

It should be noted that, despite numerous defects in the structure of the charge ordering, the stripes in the same grain at low temperatures have identical directions (except for twin orientations in grains containing twins), even though they are wavy in shape. Apparently, this fact directly indicates that the transition to the charge-ordered state is correlated in nature.

As was noted in [23, 24, 35], elastic interactions associated with the Jahn–Teller distortions of the environment of Mn^{3+} ions are responsible for the formation of the stripe superstructure with charge and orbital ordering. Most likely, repulsive forces act between the structural units formed predominantly by chains of Mn^{3+} Jahn–Teller ions and the structural units composed of chains consisting of Mn^{4+} non-Jahn–Teller ions and prevent their coalescence. According to [35], the charge ordering temperature T_{CO} is governed by the competition between the mean field induced by Jahn–Teller ions and the temperature factor kT. A decrease in the concentration of Mn^{3+} Jahn–Teller ions due to their replacement by Fe^{3+} non-Jahn–Teller ions leads to a decrease in the mean field and, as a result, in the charge ordering temperature T_{CO}. It seems likely that this is the main factor responsible for the observed decrease in the temperature T_{CO} upon doping with iron.

4. CONCLUSIONS

Thus, we investigated the evolution of the electron diffraction patterns of the initial compound $La_{0.33}Ca_{0.67}MnO_3$ and the iron-doped compound $La_{0.33}Ca_{0.67}Mn_{0.95}Fe_{0.05}O_3$ in the temperature range 91–300 K and the high-resolution lattice images of these compounds at low temperatures. The results of the analysis have demonstrated that the first peak observed at T_{CO} in the temperature dependence of the magnetization M for the $La_{0.33}Ca_{0.67}MnO_3$ and $La_{0.33}Ca_{0.67}Mn_{0.95}Fe_{0.05}O_3$ compounds upon a decrease in temperature from room temperature corresponds to a structural transition accompanied by the formation of a

superstructure. At temperatures $T < 200$ K, the superstructure formed in the undoped sample is commensurate to the initial crystal structure such that the unit cell of the superstructure $\langle\langle 3a_p\sqrt{2} \times a_p\sqrt{2} \times 2a_p\rangle\rangle$ is triple the unit cell of the initial structure. This corresponds to the vector $\mathbf{q} = 1/3\mathbf{a}^*$ in reciprocal space. The doping of the initial sample with 5 at. % Fe leads to a decrease in the temperature T_{CO} by 50 K and to the formation of the incommensurate superstructure, in which the magnitude of the vector $\mathbf{q}$ is approximately 15% less. According to the high-resolution electron microscopic data obtained at $T = 91$–92 K, the unit cell of the superstructure in the iron-doped $La_{0.33}Ca_{0.67}Mn_{0.95}Fe_{0.05}O_3$ compound is not triple the unit cell but involves defects of ordering, such as quadrupling of the unit cell, numerous translations by $a_p\sqrt{2}$ along the $\mathbf{a}$ direction, and dislocation-type defects in the stripe structure of the charge ordering. These pseudoperiodic defects result in a decrease in the magnitude of the vector $\mathbf{q}$ and are responsible for the incommensurability of the structure. The observed decrease in the magnitude of the vector $\mathbf{q}$ (by ~15%) is in good agreement with the decrease in the $Mn^{3+} : Mn^{4+}$ ratio by 15% due to the substitution of Fe^{3+} ions for Mn^{3+} ions. A decrease in the concentration of Mn^{3+} Jahn–Teller ions as a result of their replacement by Fe^{3+} isovalent non-Jahn–Teller ions brings about a substantial suppression of the charge ordering. This suggests that the Jahn–Teller effects, most likely, play a decisive role in the charge ordering in the compounds under investigation.

ACKNOWLEDGMENTS

REFERENCES

1. *Colossal Magnetoresistance, Charge Ordering, and Related Properties of Manganese Oxides*, Ed. by C. N. R. Rao and B. Raveau (World Scientific, Singapore, 1998).
2. J. Cocy, M. Viret, and S. Molnar, Adv. Phys. **48**, 167 (1999).
3. M. B. Salamon and M. Jaime, Rev. Mod. Phys. **73**, 583 (2001).
4. Yu. A. Izyumov and Yu. N. Skryabin, Usp. Fiz. Nauk **171** (2), 121 (2001) [Phys. Usp. **44** (2), 109 (2001)].
5. S. M. Dunaevskiĭ, Fiz. Tverd. Tela (St. Petersburg) **46** (2), 193 (2004) [Phys. Solid State **46** (2), 193 (2004)].
6. C. Zener, Phys. Rev. **82**, 403 (1951).
7. P. W. Anderson and H. Hasegawa, Phys. Rev. **100**, 675 (1955).
8. A. J. Miller, B. I. Shraiman, and R. Mueller, Phys. Rev. B: Condens. Matter **54**, 5389 (1996).
9. E. L. Nagaev, *Colossal Magnetoresistance and Phase Separation in Magnetic Semiconductors* (Imperial College Press, London, 2002).
10. E. Dagotto, H. Hotta, and A. Moreo, Phys. Rep. **344**, 1 (2001).
11. J. P. Goodenouph, Phys. Rev. **100**, 564 (1955).
12. P. Schiffer, A. Ramirez, W. Bao, and S. W. Cheong, Phys. Rev. Lett. **75**, 3336 (1995).
13. A. P. Ramirez, P. Schiffer, C.-W. Cheong, C. H. Chen, W. Bao, T. T. H. Palastra, P. L. Gammel, D. J. Bishop, and B. Zegarski, Phys. Rev. Lett. **76**, 3188 (1996).
14. E. O. Wollan and W. C. Koehler, Phys. Rev. **100**, 45 (1955).
15. C. H. Chen and S.-W. Cheong, Phys. Rev. Lett. **76**, 4042 (1996).
16. C. H. Chen, S.-W. Cheong, and H. Y. Hwang, J. Appl. Phys. **81**, 4326 (1997).
17. G. van Tendeloo, O. I. Lebedev, M. Herview, and B. Raveau, Rep. Prog. Phys. **67**, 1315 (2004).
18. W. Schuddinck, G. Van Tendeloo, C. Martin, M. Hervieu, and B. Raveau, J. Alloys Compd. **333**, 13 (2002).
19. A. Barnabe, A. Maignan, M. Hervieu, F. Dainay, C. Martin, and B. Raveau, Appl. Phys. Lett. **71**, 26 (1997).
20. B. Raveau, A. Maignan, C. Martin, and M. Hervieu, J. Solid State Chem. **130**, 162 (1997).
21. T. Sudyoadsuk, R. Suryanarayanan, P. Winotai, and L. E. Wenger, J. Magn. Magn. Mater. **278**, 96 (2004).
22. M. Roy, J. F. Mitchell, A. P. Ramirez, and P. Schiffer, J. Phys.: Condens. Matter. **11**, 4843 (1999).
23. S. Mori, C. H. Chen, and S.-W. Cheong, Nature (London) **392**, 473 (1998).
24. V. M. Loktev and Yu. G. Pogorelov, Fiz. Nizk. Temp. (Kharkov) **26** (3), 231 (2000) [Low Temp. Phys. **26** (3), 171 (2000)].
25. Y. Tokura, H. Kuwahara, Y. Moritomo, Y. Tomioka, and A. Asamitsu, Phys. Rev. Lett. **76**, 3184 (1996).
26. Y. Tomioka, A. Asamitsu, Y. Moritomo, H. Kuwahara, and Y. Tokura, Phys. Rev. Lett. **74**, 5108 (1995).
27. S. B. Ogale, R. Shreekala, Ravi Bathe, S. K. Date, S. I. Patil, B. Hannoyer, F. Petit, and G. Marest, Phys. Rev. B: Condens. Matter **57**, 7841 (1998).
28. K. H. Ahn, X. W. Wu, K. Liu, and C. L. Chien, Phys. Rev. B: Condens. Matter **54**, 15299 (1996).
29. R. Laiho, K. G. Lisunov, E. Lähderanta, J. Salminen, M. A. Shakhov, V. S. Stamov, P. A. Petrenko, and V. S. Zakhvalinskii, J. P Mhys. Chem. Solids **64**, 1573 (2003).
30. P. Levy, L. Granja, E. Indelicato, D. Vega, G. Polla, and F. Parisi, J. Magn. Magn. Mater. **226–230**, 794 (2001).
31. M. C. Wu, J. Chen, and X. Jin, Physica C (Amsterdam) **276**, 132 (1997).
32. P. G. Radeaelli, D. E. Cox, L. Capogna, S.-W. Cheong, and M. Marezio, Phys. Rev. B: Condens. Matter **59**, 14440 (1999).
33. M. R. Ibarra, J. M. de Teresa, J. Blasco, P. A. Algarabel, C. Marquina, J. Garcia, J. Stankiewicz, and C. Ritter, Phys. Rev. B: Condens. Matter **56**, 8252 (1997).
34. M. Jaime, M. B. Salomon, M. Rubinstein, R. E. Treece, J. S. Horwitz, and D. B. Chrisey, Phys. Rev. B: Condens. Matter **54**, 11914 (1996).
35. T. S. Orlova, J. Y. Laval, P. Monod, J. G. Noudem, V. P. Zahvalinskii, V. S. Vikhnin, and Yu. P. Stepanov, J. Phys.: Condens. Matter. **18**, 6729 (2006).

Translated by O. Borovik-Romanova